Nanoindentation Characterization of Lead-free Solders and Intermetallic Compounds under Thermal Aging

Tong Jiang[1], Fubin Song[2], Chaoran Yang[2] and S. W. Ricky Lee[1,2]
[1]Department of Mechanical Engineering
[2]Center for Advanced Microsystems Packaging
Hong Kong University of Science and Technology
Clear Water Bay, Kowloon, Hong Kong

Abstract

The enforcement of environmental legislation is pushing electronic products to take lead-free solder alloys as the substitute of traditional lead-tin solder alloys. Applications of such alloys require a better understanding of their mechanical behaviors. The mechanical properties of the lead-free solders and IMC layers are affected by the thermal aging. The lead-free solder joints on the pads subject to thermal aging test lead to IMC growth and cause corresponding reliability concerns. In this paper, the mechanical properties of the lead-free solders and IMCs were characterized by nanoindentation. Both the Sn-rich phase and Ag_3Sn + β-Sn phase in the lead-free solder joint exhibit strain rate depended and aging soften effect. When lead-free solder joints were subject to thermal aging, Young's modulus of the (Cu, Ni)$_6Sn_5$ IMC and Cu_6Sn_5 IMC changed in very small range. While the hardness value decreased with the increasing of the thermal aging time.

Key words: Lead-free solder, intermetallic compound, nanoindentation, thermal aging

Introduction

The enforcement of environmental legislation to replace lead based solders in electronic products has resulted in a lot of studies on lead-free solders. The leading candidates of lead-free solders include binary and ternary alloys based on the SnCu and SnAg alloy systems, in near eutectic alloy forms. This includes a class of near-eutectic SnAgCu (SAC) alloys that provide acceptable electrical and mechanical properties [1, 2]. During reflow processing for electronic interconnections, the formation of IMC at solder/substrate interface is inevitable for the joining action. However, during storage and usage, the growth of IMCs will influence the reliability of solder joints. It has been identified that fracturing around the interfacial IMC layer is the primary failure induced by drop impacts in particular for lead-free solder joints [3-6]. Therefore, characterizations of mechanical properties of lead-free solders and IMCs in the structural and mechanical properties have attracted great interests [7-16].

Nanoindentation has received a great deal of attention for probing the mechanical behavior of materials at extremely small scales, which also has an ability to measure the properties of materials in thin films. The nanoindentation hardness, Young's modulus can be calculated from the load-displacement curve using Oliver and Pharr method [17, 18]. In real applications, the thickness of the IMC layer is in the range of a few microns and the IMC particles are under micron in dimension [19]. Thus, nanoindentation is suited for the investigation of mechanical property of IMC material. Some researchers have already reported the mechanical properties of eutectic/near eutectic SnAg or SAC alloys and IMC materials [7-16]. However, the data collected from the real solder joints are very rare. Therefore, the nanoindentation mechanical properties of lead-free solder joints and IMCs should be investigated in detail.

In the current study, the real solder joints on two different pad finishes were fabricated for the nanoindentation test. The nanoindentation mechanical properties of individual phases in the lead-free solder joints and interfaces were studied after thermal aging tests. Nanoindentation test was used to probe the Young's modulus and hardness of the lead-free solder and IMC material, respectively. The effects of the strain rate and the thermal aging on the mechanical properties were also investigated.

Table. 1 Test matrix of lead-free solder joints

Sample Number	Solder Joint	Pad Finish	Reflow Peak Temperature
1	SAC105	OSP	255°C
2	SAC305	OSP	245°C
3	SAC387	OSP	245°C
4	SAC105	ENIG	255°C

Experiment Procedure

The lead-free solder alloys used in this study were Sn3.8%Ag0.7%Cu (SAC387), Sn3.0%Ag0.5%Cu (SAC305), and Sn1.0%Ag0.5%Cu (SAC105). The packages were fabricated using 0.76 mm diameter solder spheres with solder pastes attached on organic solder preservative (OSP) and electroless-nickel immersion gold (ENIG) pad finishes. The pad opening was 0.63 mm diameter with solder-mask-defined.

The SAC solder spheres were attached to the package substrate pad with the solder alloy pastes. The stencil thickness used for the solder paste print was 0.12 mm. Table 1 shows the solder joint matrix.

After solder spheres attachment, except for those kept as base case reference, all specimens were put in an oven for thermal aging at 125˚C. The thermal aging test continued for 1000 hours and some samples were removed from the oven at 500 and 1000 hours. For the IMC analysis, the selected testing samples were molded after aging test, cross-sectioned and etched (2% HCl + 98% methanol). After selective deep etching to remove the Sn phase, the IMC layer was exposed for investigation.

The nanoindentation test was performed on a Triboindenter (Hysitron, USA). A Berkovich diamond indenter of tip was used during the test. The resolutions of the loading and displacement of the systems were 1 nN and 0.0002 nm, respectively. All the nanoindentation tests were conducted at room temperature. For each indentation test on SAC solder joint, a 7×7 grid array was designed to ensure the spacing among the indents. The maximum load was 5000 nN prescribed on the different phase. The dwell time during the test was 5 s. The Berkovich indenter was pressed into the sample surface with a constant loading rate. For SAC lead-free solder joint, the nanoindentation test was performed with different strain rate 0.01 s^{-1}, 0.1 s^{-1}, 1 s^{-1} and 10 s^{-1}. For IMC layer, the nanoindentation test was performed at the strain rate of 0.1 s^{-1}. Nanoindentation and in-situ imaging of the indents on individual phases were carried out using the atomic force microscopy (AFM) on the Triboindenter. After the test, the SEM was employed to identify the indentation traces.

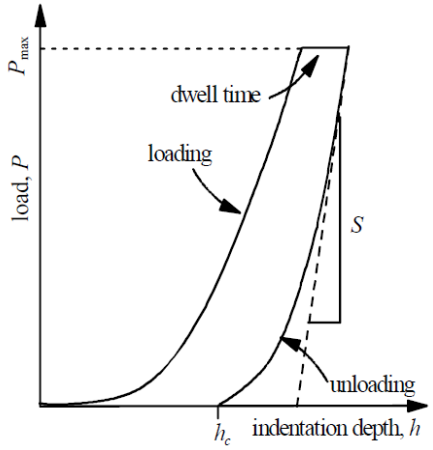

Fig. 1 Typical load and displacement curve for nanoindentation test

Results and Discussion

A typical nanoindentation testing cycle consists of three segments, loading, dwell time at target load, and unloading, as illustrated in Fig. 1. During the indentation test, the continuous force-displacement relation is recorded. The stiffness at the onset of unloading curve is used as the Young's modulus.

The Mayer's hardness for the nanoindentation test is defined as the maximum load divided by the projected area on the material, which reflects a similar physical meaning of the conventional stress [17]. Therefore, in the following analysis, the hardness, combined with the strain rate, will be utilized later to value the mechanical properties of SAC solders and IMCs.

The actual contact area A is calculated by the actual indentation displacement h_p, which is given by:

$$A = 3\sqrt{3}h_p^2 \tan^2 65.27 = 24.5h_p^2 \quad (1)$$

The Mayer's hardness is thus obtained by:

$$H = \frac{P_{\max}}{A} \quad (2)$$

The reduced modulus E_r is derived from measuring the contact stiffness at the onset of unloading curve.

$$E_r = \frac{\sqrt{\pi}}{2\beta}\cdot\frac{S}{\sqrt{A}} = \left[\frac{1-\nu^2}{E} + \frac{1-\nu_i^2}{E_i}\right]^{-1} \quad (3)$$

where E and ν denote the Young's modulus and Poisson's ratio of the indented material, respectively, while E_i and ν_i represent the parameters corresponding to the indenter, which are taken as 1140 GPa and 0.07, respectively.

The microstructure after the nanoindentation test was investigated by SEM as shown in Fig. 2. There are two phases in the SAC lead-free solder, the Sn-rich phase and Ag_3Sn + β-Sn phase. As shown in the Fig. 2(b) and (c), the mark size on the β-Sn phase is larger than the Ag_3Sn + β-Sn phase. This means that the deformation of Sn-rich phase is larger than the Ag_3Sn + β-Sn phase at the same loading condition.

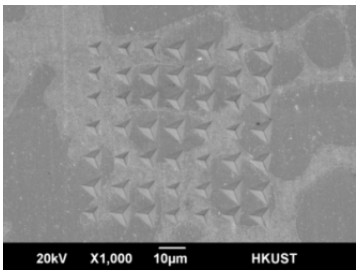

(a) Typical indentation marks on SAC lead-free solder joint

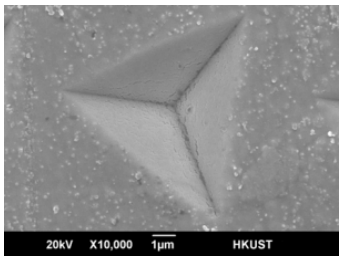

(b) Mark on Sn-rich phase

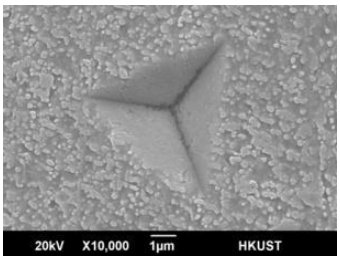

(c) Mark on Ag_3Sn+β-Sn phase

Fig. 2 Typical indentation marks on SAC lead-free solder joint

Fig. 3 shows typical load-displacement results obtained with 5000nN maximum load indentations at different strain rates. For test of the same maximum load, the maximum indentation depth for SAC lead-free solder is much deeper than that of IMC. The SAC solder is found to be very soft and exhibited significant plasticity both on Sn-rich phase and Ag_3Sn + β-Sn phase. Upon unloading, the solder recovers only very less than the indentation depth before the unloading. In contrast to the solder, the IMCs are significantly harder with less indentation depth. The curve for $(Cu, Ni)_6Sn_5$ IMC has less depth comparing the Cu_6Sn_5 IMC. The IMC typically recovers around 25% of the maximum penetration of the indenter after unloading. From this, the deformation of the intermetallic phases is found to be both elastic and plastic, while the deformation of the solder is found to be primarily plastic.

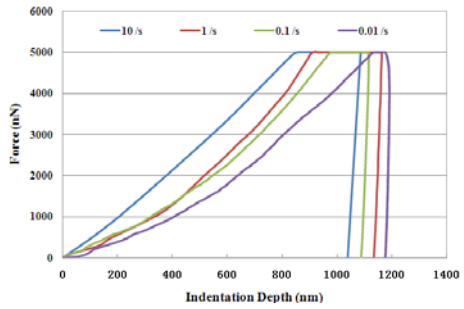

(a) Sn-rich phase

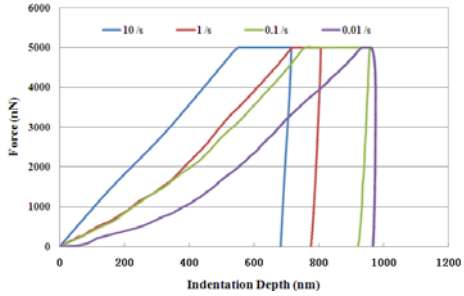

(b) Ag_3Sn+β-Sn phase

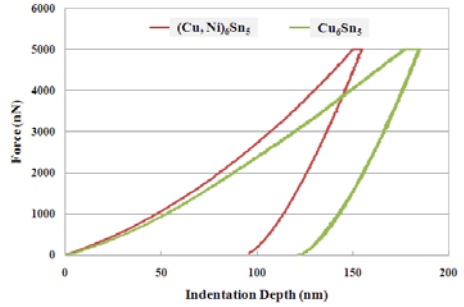

(c) IMC

Fig. 3 Load and displacement curves of nanoindentation test

The AFM images of residual indents show the differences between the lead-free solders and the IMCs. The phases in lead-free solder exhibit pile-up behaviors, as seen in Fig. 4 (a) and (b). The SAC lead-free solder has larger plastic deformation under the same loading condition comparing to the IMC. The residual indents observed for $(Cu, Ni)_6Sn_5$ and Cu_6Sn_5 exhibite smooth profiles with less detected pile-up of materials as shown in Fig. 4 (c) and (d).

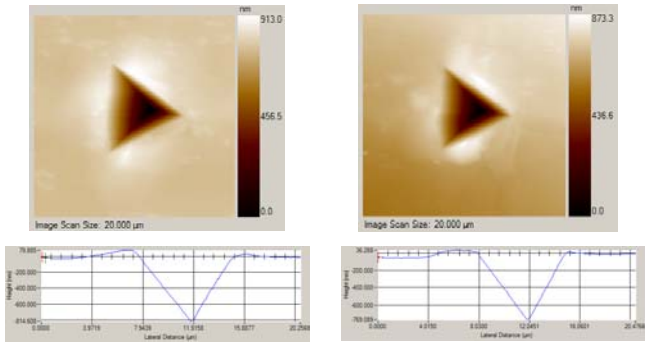

(a) Sn-rich phase (b) Ag_3Sn+β-Sn phase

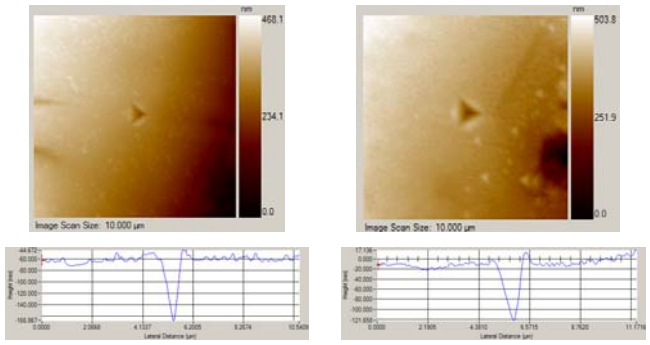

(c) $(Cu, Ni)_6Sn_5$ (d) Cu_6Sn_5

Fig. 4 Atomic force microscopy images and height profiles

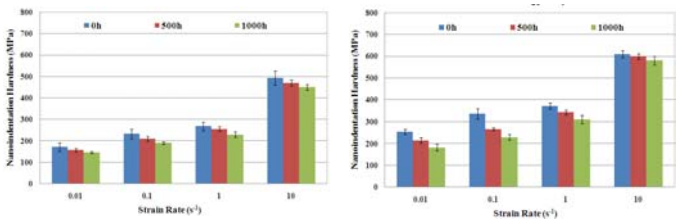

(a) SAC105 Sn-rich phase (b) SAC105 Ag_3Sn + β-Sn

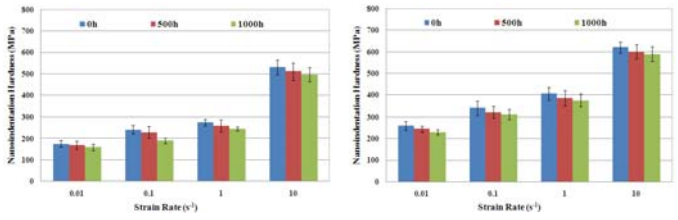

(c) SAC305 Sn-rich phase (d) SAC305 Ag_3Sn + β-Sn

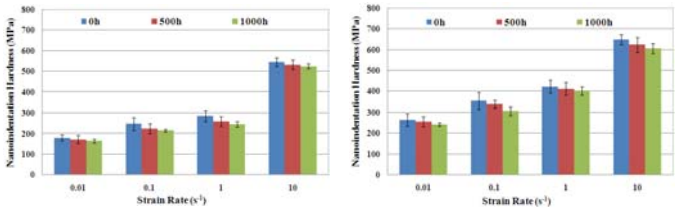

(e) SAC387 Sn-rich phase (f) SAC305 Ag_3Sn + β-Sn

Fig. 5 Comparisons of nanoindentation hardness of the SAC lead-free solder joints

The Fig. 5 shows the summary of nanoindentation tests on the two different phases of three SAC lead-free solder joints. For all the SAC lead-free solders, both nanoindentation hardness of two phases increase with the increasing of the strain rates. The hardness at the stain rate of 10 s^{-1} is almost three times of that at the strain rate 0.01 s^{-1}. This shows the strain rate effects both on the Sn-rich phase and Ag_3Sn + β-Sn phase. For the thermal aging effect, the nanoindentation hardness decreases as the thermal aging time increase. That means both the Sn-rich and Ag_3Sn + β-Sn phases become softer after thermal aging. When comparing these three different lead-free solders at the same strain rate and aging hour, not too much difference is found for Sn-rich phase. For the Ag_3Sn + β-Sn phase, the hardness value of SAC387 is little higher than those of SAC305 and SAC105.

Fig. 6 and Fig. 7 provide SEM micrographs of the IMC layers for representative test samples at 0, 500 and 1,000 hours of thermal aging. Based on SEM observations and qualitative EDX analysis, the initial intermetallic phase is primarily Cu_6Sn_5 on as-reflowed samples with OSP pad finishes and (Cu, $Ni)_6Sn_5$ with ENIG pad finishes. After continued thermal exposure, the Cu_6Sn_5 changed morphologically into layer-type. The thickness of the (Cu, $Ni)_6Sn_5$ and Cu_6Sn_5 IMC layers are also increasing with the increasing of thermal aging. The thickness of (Cu, $Ni)_6Sn_5$ IMC layer is thinner than Cu_6Sn_5 IMC layer.

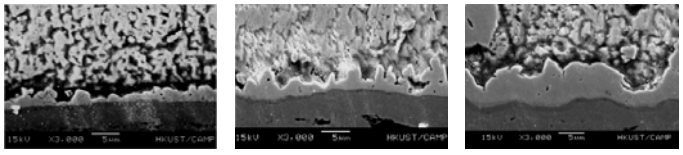

(a) 0 hour (b) 500 hours (c) 1000 hours

Fig. 6 IMC growth and morphology changes subject to thermal aging at 125˚C (OSP)

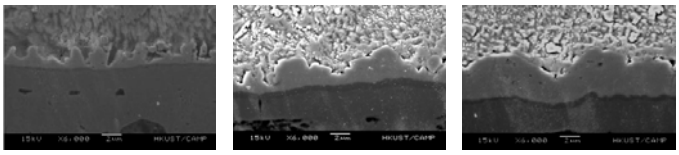

(a) 0 hour (b) 500 hours (c) 1000 hours

Fig. 7 IMC growth and morphology changes subject to thermal aging at 125˚C (ENIG)

The SEM and EDX analysis of nanoindentation marks on (Cu, $Ni)_6Sn_5$ and Cu_6Sn_5 IMCs are shown in Fig. 8. Comparisons of the Young's modulus and nanoindentation hardness for the IMCs subjected to thermal aging are shown in Fig. 9 and 10. Although the IMC layers grow in thickness during thermal aging tests, no significant change in the Young's modulus is found. The Young's modulus of (Cu, $Ni)_6Sn_5$ IMC is 146 GPa for as reflowed solder joint and 144.8 after 1000 hours thermal aging. The Young's modulus of (Cu, $Ni)_6Sn_5$ IMC shows higher value than the Cu_6Sn_5 IMC. The Young's modulus of Cu_6Sn_5 IMC is 116.52 GPa for as reflowed solder joint and 115 GPa after 1000 hours thermal aging. The nanoindentation hardness of the IMC layers decreases with the increasing of the thermal aging time. The (Cu, $Ni)_6Sn_5$ IMC has the higher nanoindentation hardness value than Cu_6Sn_5 IMC. The nanoindentation hardness of (Cu, $Ni)_6Sn_5$ IMC is 10.85 GPa after the reflow and that of Cu_6Sn_5 IMC is 6.7 GPa. After 1000 hours aging time, the hardness of (Cu, $Ni)_6Sn_5$ IMC decreases to 9.91 GPa and that of Cu_6Sn_5 IMC decreased to 6.28 GPa.

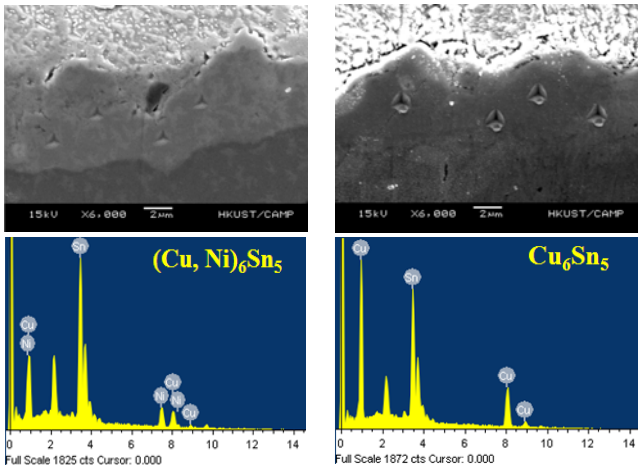

(a) (Cu, $Ni)_6Sn_5$ IMC (b) Cu_6Sn_5 IMC

Fig. 8 SEM and EDX analysis of IMCs

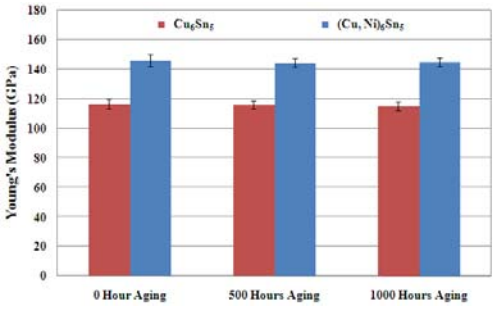

Fig. 9 Young's modulus of IMCs subject to thermal aging time at 125˚C

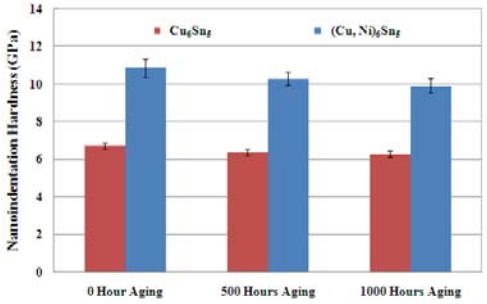

Fig. 10 Nanoindentation hardness of IMCs subject to thermal aging time at 125˚C

Conclusions

The mechanical properties of SAC lead-free solder joints and IMCs were investigated by nanoindentation tests. The individual phases in the SAC lead-free solder joints, Cu_6Sn_5, and (Cu, $Ni)_6Sn_5$ IMCs were analyzed. The effects of different

loading and unloading strain rates, varying from 0.01 to 10 s^{-1} on nano mechanical responses of the SAC lead-free solder joints were studied. The thermal aging effect on the lead-free solder joints and IMCs were also investigated. The larger pile-up was observed on both Sn-rich phase and Ag_3Sn + β-Sn phase while less pile-up effect for (Cu, Ni)$_6Sn_5$ and Cu_6Sn_5 IMCs. The hardness of the SAC lead-free solder joints were obviously strain rate dependent. The nanoindentation hardness of SAC lead-free solders decreased with increasing of aging time. For the two types of IMCs, the (Cu, Ni)$_6Sn_5$ IMC had higher nanoindentation hardness value than the Cu_6Sn_5 IMC. Although the IMC layers grew in thickness during thermal aging tests, no significant change was found in the Young's modulus. The nanoindentation hardness of the (Cu, Ni)$_6Sn_5$ and Cu_6Sn_5 IMC decreased with the increasing of the thermal aging time.

Acknowledgments

This study was supported by Research Grants Council of Hong Kong through a General Research Fund project #615208 to the Hong Kong University of Science and Technology. The authors wish to acknowledge this support.

References

1. M. Abtew, G. Selvaduray, "Lead Free Solders in Microelectronics," *Material Science & Engineering*, 27(2000), pp. 95-141.
2. John W. Evans. A Guide to Lead-free Solders. Springer, 2007.
3. E.H.Wong, R. Rajoo, Y.-W. Mai, S.K.W. Seah, K.T. Tsai, L.M. Yap, "Drop Impact: Fundamentals and Impact Characterization of Solder Joints," *Proc 55th Electronic Components and Technology Conference*, Lake Buena Vista, FL, USA, (2005), pp. 1202-1209.
4. Ahmer Syed *et al*., "Effect of Pb-free Alloy Composition on Drop/Impact Reliability of 0.4, 0.5 & 0.8mm Pitch Chip Scale Packages with NiAu Pad Finish," *Proc 57th Electronic Components and Technology Conference*, Reno, NV, (2007), pp. 951-956.
5. Fubin Song, S. W. Ricky Lee, Keith Newman, Bob Sykes, Stephen Clark, "Brittle Failure Mechanism of SnAgCu and SnPb Solder Balls during High Speed Ball Shear and Cold Ball Pull Tests," *Proc 57th Electronic Components & Technology Conference*, Reno, NV, (2007), pp. 364-372.
6. Fubin Song, S. W. Ricky Lee, Keith Newman, Bob Sykes, Stephen Clark, "High-Speed Solder Ball Shear and Pull Tests vs. Board Level Mechanical Drop Tests: Correlation of Failure Mode and Loading Speed," *Proc 57th Electronic Components & Technology Conference*, Reno, NV, (2007), pp. 1504-1513.
7. Yong Sun *et al*., "Nanoindentation for Measuring Individual Phase Mechanical Properties of Lead-free Solder Alloy," *Mater. Sci*. *Mater Electron* (2008) 19, pp. 514-521.
8. Feng Gao *et al*., "Mechanical Properties Versus Temperature Relation of Individual Phases in Sn-3.0Ag-0.5Cu Lead-free Solder Alloy," *Microelectronics Reliability,* 49 (2009), pp. 296-302.
9. R.R. Chromik, R.P. Vinci, S.L. Allen, M.R. Notis, "Nanoindentation Measurements on Cu-Sn and Ag-Sn Intermetallics Formed in Pb-free Solder Joints," *J. Mater. Res.* 18 (9) (2003), pp. 2251-2261.
10. H.-J. Albrecht, A. Juritza, K.M¨uller,W.H.M¨uller, J. Sterthaus, J.Villain, A. Vogliano, "Interface Reactions in Microelectronic Solder Joints and Associated Intermetallic Compounds: an investigation of their mechanical properties using nanoindentation," *Proc 5th Electronics Packaging Technology Conference*, Singapore, (2003), pp. 726-731.
11. X. Deng, M. Koopman, N. Chawla, K.K. Chawla, "Young's Modulus of (Cu,Ag)-Sn Intermetallics Measured by Nanoindentation," *Mater. Sci. Eng.* A 364 (2004), pp. 240-243.
12. X. Deng, N. Chawla, K.K. Chawla, M. Koopman, "Deformation Behavior of (Cu,Ag)-Sn Intermetallics by Nanoindentation," *Acta Mater.* 52 (14) (2004), pp. 4291-4303.
13. G.-Y. Jang, J.-W. Lee, J.-G. Duh, "The Nanoindentation Characteristics of Cu_6Sn_5, Cu_3Sn, and Ni_3Sn_4 Intermetallic Compounds in the Solder Bump," *J. Electron. Mater.* 33 (10) (2004), pp.1103-1110.
14. L. Xu, J.H.L. Pang, "Nano-indentation Characterization of Ni-Cu-Sn IMC Layer Subject to Thermal Aging," *Thin Solid Films,* 504 (2006), pp.362-366.
15. Z. Chen, M. He, B. Balakrisnan, C.C. Chum, "Elasticity Modulus, Hardness and Fracture Toughness of Ni_3Sn_4 Intermetallic Thin Films," *Mater. Sci. Eng*. A 423 (2006), pp. 107-110.
16. Ping-Feng Yang *et al*., "Nanoindentation Identifications of Mechanical Properties of Cu_6Sn_5, Cu_3Sn, and Ni_3Sn_4 Intermetallic Compounds Derived by Diffusion Couples," *Mater. Sci. Eng.* A 485 (2008), pp. 305-310
17. W.C. Oliver and G.M. Pharr, "An Improved Technique for Determining Hardness and Elastic Modulus Using Load and Displacement Sensing Indentation Experiments," *J Mater Res* 7(6), (1992), pp. 1564-83.
18. W.C. Oliver *et al*., "Measurement of Hardness and Elastic Modulus by Instrumented Indentation," *J. Mater. Res.*, Vol. 19, No. 1, (2004).
19. K. Zeng and K. N. Tu, "Six Cases of Reliability Study of Pb-free Solder Joints in Electronic Packaging Technology," *Mater. Sci. Eng. R*, vol. 38, No. 2 (2002), pp. 55-105.